

A single-span aeroelastic model of an overhead electrical power transmission line with guyed lattice towers

W.E. Lin ^a, E. Savory ^a, R.P. McIntyre ^a, C.S. Vandelaar ^b and J.P.C. King ^c

The University of Western Ontario, London, Ontario, Canada

^a*Department of Mechanical & Materials Engineering, wlin26@uwo.ca,*

esavory@eng.uwo.ca and rmcinty2@uwo.ca

^b*University Machine Services, cvandela@uwo.ca*

^c*Alan G. Davenport Wind Engineering Group, jpck@blwtl.uwo.ca*

1 INTRODUCTION

The typical method of high-voltage electricity transmission uses conductors that are carried above ground by towers. Kiessling et al. (2003) provided a comprehensive description of overhead transmission line technology. Existing design practices have been documented (ASCE, 1991; 1992). Support structures are generally designed to be as lightweight as possible to minimize the cost of carrying lines over distances of, say, hundreds of kilometres with a support structure at every half-kilometre.

The present study considers a half-span of lines on either side of the support tower. The tower is kept vertical solely by the resistance from steel cables under tension (i.e. guy wires). For their spatial extent and compared to most engineered structures, transmission lines are relatively low in mass and potentially high in stiffness. Thus, it may be expected that this type of structure is susceptible to excitation by wind. In particular, utility companies and other concerned parties (Langlois, 2006; McCarthy and Melsness, 1996) have documented the failure of transmission line systems from downdraft wind loads.

Previous investigators have studied wind loading of the individual components of a transmission line, as well as the system as a whole. Loredou-Souza and Davenport (1998) discussed some aspects of the problem of line behaviour in strong winds. In particular, galloping of lines has attracted attention from researchers (e.g. Macdonald et al., 2008).

Wind loading of guyed lattice structures has been extensively studied, particularly for telecommunications masts of hundreds of metres in height, which are guyed at multiple levels. Irvine (1981) presented a unified account of cable structures with emphasis on theoretical aspects of the response of cables under load. Madugula (2002) provided a survey of research on the dynamic response of lattice structures with emphasis on practical design. Guyed mast and lattice tower structures have recently been aeroelastically modelled by Zhu (2007) and Kong et al. (2009), respectively.

The transmission line system of interest, in the present study, has been numerically modelled by Shehata et al. (2005) and Shehata and El Damatty (2007; 2008). The section of the line that failed on 5 September 1996 near Grosse Isle, Manitoba, Canada was exposed to an eastward-moving storm system (McCarthy and Melsness, 1996). The scope of this study was to design and test a physical model of this line section that failed due to downdraft outflow winds. The aeroelastic model was designed for exposure, in a single wind tunnel facility, to wind loading from (1) a conventional atmospheric boundary-layer and (2) a downdraft outflow. Section 2 describes the full-scale transmission line system that was modelled. Section 3 describes the design and construction of the aeroelastic model. Section 4 presents the simulation results. Section 5 delivers conclusions from the simulation results.

2 FULL-SCALE SYSTEM

The vertical tower shaft extended 44.4 m above foundation level (AFL) and was assembled from seven sections. The tower had a pinned base; the rectangular lattice converged upon a spherical annular bearing that was centred about a vertical pin. This base condition eliminated bending effects through the foundation, but provided limited resistance against rotation about the vertical axis of the tower.

Two horizontal cross-arms of lattice construction protruded from the vertical tower shaft. At 35.2 m AFL, on both sides of the tower, a cross-arm extended transverse to the main vertical shaft centreline, terminating at the attachment location for two guy wires that connect with the ground. At 38.2 m AFL, on both sides of the tower, a cross-arm extended transverse to the main vertical shaft centreline, terminating at the attachment location where an insulator string and a conductor pair are slung below. The conductor cross-arm is orthogonal to the guy wire cross-arm.

Between the ground anchor and the tower cross-arm tip, the sag-to-span ratio of the guy wires was 1:588. The discrepancy between the true catenary form and a straight-line approximation was minimal, so the latter value was used in the model design. Galvanized steel guy wires of 0.0117 m (0.460") diameter resisted horizontal displacement of the tower and introduced an initial compression of its main vertical legs. Two guy wires were attached to each of the two ends of the guy cross-arm at locations that were 3.05 m transverse from the main vertical shaft centreline and 35.2 m AFL. The ground anchor arrangement positioned the guy wires at 28° from vertical and 45° from the guy cross-arm axis in plan. A twin guying design was employed - each guy wire formed a pulley and was looped through a sheave at the ground anchor and a sheave at the guy cross-arm. The straight chord length of a guy wire loop was 44.4 m.

Conductors were suspended beneath each end of the larger cross-arm. Each tower carried a bundled conductor pair. The conductors may swing as a pendulum below the cross-arm, up to a maximum allowable angle of 30° from vertical. The conductor diameter was 0.04064 m and the wire construction used a steel core within a jacket of aluminium strands. The mass per unit length of a conductor was 2.897 kg/m. The modulus of elasticity was 62.7 GPa after prolonged service. The straight-line distance between towers was 488 m. The line tension was approximately 40 kN.

3 AEROELASTIC MODEL

The model is comprised of the following components: (1) a lattice tower, (2) four guys that support the tower at a single height, and (3) a half-span of lines on either side of the tower. The tower was located at mid-span with a half-span of lines on either side of the tower. The test facility span was 2.44 m compared to a full-scale distance between adjacent towers of 488 m. Thus, a single-span model at zero yaw ($\phi = 0$) to the wind tunnel flow would have a geometric scaling of 1:200. At non-zero yaw, with the wind tunnel diagonal in plan being larger than 2.44 m, a larger geometric scaling was possible. At $\phi = 60^\circ$, the diagonal corresponds to a geometric scaling of 1:100. Rather than modelling an identical line segment at various yaws at different geometric scaling, distorted horizontal length scaling (Loredo-Souza and Davenport, 2001) was applied to the lines to obtain 1:100 geometric scaling at all yaw angles. Table 1 shows the resulting scaling ratios of physical parameters of interest.

Strain gauges in Wheatstone bridge circuits were fixed on the mast spine at two heights as shown in Figure 1, in order to provide an indication of bending moments. Strain gauges were mounted on the cantilevered end springs for both the upstream and downstream conductor lines to provide an indication of the variation of conductor tension during wind loading.

The transmission line model was tested with a boundary layer wind load and then with a downdraft outflow wind load. Savory et al. (1992) conducted boundary layer simulations in the wind tunnel of interest with a target length scaling of 1:100. Full-scale equivalent aerodynamic roughness height (z_0) and gradient height (z_g) were reported as 0.0423 m and 329 m, respectively. ASCE (1999; p. 58) Class 3 open flat terrain with grass and few isolated obstacles is described with $z_0 = 0.03$ m and $z_g = 275$ m. The wind tunnel was subsequently converted to downdraft outflow simulation mode (Lin and Savory, 2010) with the tower mast positioned at 15 slot heights downstream of the slot exit. The transient flow was generated by a secondary fan set at constant speed and a gate that was rapidly opened and shut. The simulator settings were adjusted such that the normal-to-line peak wind speed at model conductor height was as close to 7 m/s as possible. The gate actuation was monitored with a potentiometer. The transient front was detected with a single hot-wire probe located at one slot height downstream of the model, quarter-span and conductor height. The following section discusses the results for zero yaw.

4 RESULTS

4.1 Aeroelastic model response to atmospheric boundary layer wind loading

The boundary layer wind speeds were set and measured with three pitot-static tube probes. One probe was roof-mounted at a height (z) of 1.46 m, on the tunnel centreline and downstream of the line model by 16 % of the line span (S). The other two probes were floor-mounted at the highest ($z = 0.345$ m) and lowest ($z = 0.145$ m) conductor heights. These two probes were slightly off the tunnel centreline (by $0.04 \cdot S$) and downstream of the line model (by $0.18 \cdot S$).

Tower bending moments were recorded with the instrumentation described in Section 3. The sign conventions for positive bending moment are indicated in Figure 1. The following presentation focuses on the along-wind tower moment (M_{yy}).

Figure 2 shows the wind speed and tower response spectral density (S_{uu} and S_{mm}) determined by spectral estimation from the fluctuating component of their respective histories. Resonant dynamic response can be distinguished from the background response (m_B^2). The mean-square fluctuating response in the first resonant mode of vibration ($m_{R,1}^2$) is shown as the filled area in the figure. Figure 3 shows that the background response increases with mean wind pressure. The approximately linear relationship supports the expected quasi-static response of the aeroelastic model to a boundary layer wind load.

Table 2 summarizes the contributions of the background and first resonant mode, relative to the total response (m_T^2). Generally, the background component contributes about a quarter of the total response and the first resonant mode contributes up to half of the total response. The first resonant mode contribution to the total response exhibits a consistently decreasing trend with increasing mean wind speed. The first resonant mode has an approximate bandwidth of 3 Hz, centred at a frequency of 5 Hz. Its bandwidth widens slightly (by about 1 Hz) and the resonant peak is centred at a slightly higher frequency (around 6 Hz). These trends are also apparent from Figure 2.

The spectral content of the axial forces on the conductors were examined based on records from the line end gauging described in Section 3. All of the axial force spectra from boundary layer wind forcing of the upstream conductor included a peak at 5 to 6 Hz (centre frequency increases with mean wind speed). All of the axial force spectra from boundary layer wind forcing of the downstream conductor included a peak at approximately 6 Hz. The spectral peak bandwidth was narrow (5 Hz) for both upstream and downstream conductors.

4.2 Aeroelastic model response to downdraft outflow wind loading

The downdraft outflow simulator was operated as specified in Section 3. The position of the computer-controlled slot gate was monitored with a potentiometer. The gate was fully-opened and -shut over a voltage range of 3.46 ± 0.04 V. Figure 4 is a representative realization from the ensemble of trials. The six sampled quantities shown were synchronized in time by the acquisition system that recorded data at a rate of 8183 samples per second (per channel). Figure 4(a) shows the actuation of the gust was completed in less than a second. The potentiometer output history was repeatable over the ensemble.

The downdraft outflow wind speed ($U + u$) record in Figure 4(b) was measured with a single hot-wire anemometry probe at the mean conductor height, at quarter-span and approximately one slot height downstream of the model. The following two boundary layer wind speeds are shown for comparison: the peak wind speed at the highest conductor height and the trough wind speed at the lowest conductor height (three slot heights downstream of the model and $0.04 \cdot S$ off the tunnel centreline).

The smallest and largest values in the ensemble of downdraft outflow peak ($U + u$) were 5.5 and 7.2 m/s, respectively. In comparison, the peak boundary layer wind speed at the lowest and highest conductor heights were 6.6 and 8.4 m/s, respectively. The arithmetic mean of the ensemble of downdraft outflow peak ($U + u$) at mean conductor height was 6.3 m/s. The mean boundary layer wind speed at the lowest and highest conductor heights were 5.1 and 6.7 m/s, respectively.

Each downdraft outflow wind speed record was separated into mean (U) and residual (u) components. The decomposition followed the moving average procedure described by Lin and Savory (2010). The smallest and largest values in the ensemble of downdraft outflow peak U were 4.0 and 5.4 m/s, respectively.

Spine bending moments were determined at four gauge pair sites. The gauge pairs at the lower site (see Figure 1) did not register significant transient behaviour as the gust moved past the tower, thus only the results from the gauge pairs at the upper site are shown as Figure 4(c) and (d). The x-x and y-y axes were oriented normal and parallel to the lines, respectively. The sign conventions for positive bending moment are indicated in Figure 1. The maximum and minimum bending moments from the boundary layer wind loading are shown for comparison.

Strain gauges on the line end springs gave an indication of the axial force on the upstream and downstream conductors, as shown in Figure 4(e) and (f), respectively. The sign convention was positive in the direction away from the modelled tower (i.e. increasingly positive for increasing line tension). Aside from the increased magnitude as the gust passes the conductors, the upstream conductor motion showed a noticeable periodicity of approximately 5 Hz. As discussed in Section 4.1, the conductors also predominantly vibrated at this frequency with boundary layer wind forcing.

Pertaining to Figure 4(c) to (f), the strain gauge outputs were low-pass filtered at 60 Hz. This signal processing allowed the synchronicity of the transient extremum (if present) in all six signals to be clearly identified. As well, the low-frequency components of the signals that are most significant for wind loading were drawn out.

The initial ensemble of fifty-seven downdraft outflow trials were further examined and pared down based on two criteria. First, since the anemometer is slightly downstream of the tower model, the peak in the wind speed signal should occur a fraction of a second later than the peak in the along-wind tower response signal. Five trials (9 %) had the unexpected result of the tower response peak lagging the wind speed peak by significantly greater than one second. Fifteen trials (26%) had the tower response and wind speed peaks occurring almost simultaneously (tower response peak lagged the wind speed peak by less than a third of a second). Clearly, this turbulent flow is more complex than an idealized roll vortex and the structural model was possibly sensitive to non-uniformities in the propagation of the dominant vortex. These trials warrant further study and were excluded from present consideration. Second, it has been established that a dominant vortex

causes the peak wind speed in the simulation (Lin and Savory 2010). For the remaining trials, the speed at which the dominant vortex advects can be determined from the duration by which the wind speed peak lags the tower response peak and the known distance between the tower and anemometer. Four trials (7 %) had a much larger advection speed than expected (> 6 m/s); they were excluded from further consideration. The remaining thirty-three trials (58 %) each had an advection speed in the expected range (1 to 2 m/s).

The spectral content of the near-peak duration was examined for this ensemble of thirty-three trials that met the criteria described above. The near-peak duration included one thousand samples preceding and one thousand samples following the occurrence of the peak value (i.e. approximately the half-duration as defined by Lin and Savory 2010). The most significant spectral peak occurred in the mean-square fluctuating tower response between 10 Hz and 20 Hz. The ensemble average is obtained by averaging the spectra from the thirty-three trials. Individual spectral peaks are obscured in the ensemble average, but it is clear that most of the fluctuating tower response is in the frequency range of 10 Hz to 30 Hz. By identifying a background response and resonant dynamic response, m_B^2/m_T^2 and m_R^2/m_T^2 were determined as 55 % and 45 %, respectively.

5 CONCLUSIONS

Aeroelastic modelling of a single span of a transmission line with a supporting lattice tower was achievable at a length scaling of 1:100 with distorted line scaling, with simplification of the lattice tower to an equivalent mast and by skirting the limits of what was practical in terms of model construction and wind tunnel experiment.

Spectra for the fluctuating component of both the tower response and the line response, to the boundary layer wind forcing, contained a narrowband peak at 6 Hz. This first resonant mode contributed twice as much as the background component, to the total mean-square fluctuating tower response. Most of the fluctuating tower response to downdraft outflow wind forcing was at higher frequencies (10 Hz to 30 Hz). Resonant dynamic response was less significant with downdraft outflow wind forcing than boundary layer wind forcing, because with the former, the background component had a larger contribution to the total mean-square fluctuating tower response than the resonant component.

Although there were notable resonant contributions, they did not significantly affect the quasi-static behaviour of the aeroelastic model. With boundary layer wind forcing, the background response of the tower increased linearly with mean wind pressure. With downdraft outflow wind forcing, the records from model instrumentation were closely synchronized with the wind speed record for a majority of the ensemble.

The aeroelastic transmission line model generally responded quasi-statically to both types of wind forcing. These findings do not find cause for transmission line failure from downdraft outflow winds. Further work should scrutinize the maximum instantaneous measured loads and the possible dynamic behaviour associated with the trials that were excluded from this analysis. Finally, it would be interesting to investigate full-scale response to assess whether a natural frequency of 0.6 Hz is evident, as predicted by the first resonant mode of vibration of this aeroelastic model with time scaling of 1:10.

6 REFERENCES

- American Society of Civil Engineers (ASCE), 1991. Guidelines for electrical transmission line structural loading. ASCE Manuals and Reports on Engineering Practice 74. New York, NY, USA.
- American Society of Civil Engineers (ASCE), 1992. Design of latticed steel transmission structures. Standard ANSI/ASCE 10-90. New York, NY, USA.
- American Society of Civil Engineers (ASCE), 1999. Wind tunnel studies of buildings and structures. ASCE Manuals and Reports on Engineering Practice 67. New York, NY, USA.
- Irvine, H.M., 1981. Cable structures. The MIT Press, Cambridge, MA, USA.

- Kiessling, F., Nefzger, P., Nolasco, J.F., Kaintzyk, U., 2003. Overhead power lines: planning, design, construction. Springer-Verlag, Berlin, Germany.
- Kong, L., Jeong, U.Y., Edey, R.T., King, J.P.C., 2009. A study of wind effects for Hoover Dam bypass project: full aeroelastic model study. BLWT-SS11-2009. The Boundary Layer Wind Tunnel Laboratory.
- Langlois, S., 2006. Effect of high intensity winds on overhead transmission lines. CIGRÉ WG B2.06 (05).
- Lin, W.E., Savory, E., 2010. Physical modelling of a downdraft outflow with a slot jet. Wind and Structures 13(5), 385-412.
- Loredo-Souza, A.M., Davenport, A.G., 1998. The effects of high winds on transmission lines. Journal of Wind Engineering and Industrial Aerodynamics 74-76, 987-994.
- Loredo-Souza, A.M., Davenport, A.G., 2001. A novel approach for wind tunnel modelling of transmission lines. Journal of Wind Engineering and Industrial Aerodynamics 89, 1017-1029.
- Macdonald, J.H.G., Griffiths, P.J., Curry, B.P., 2008. Galloping analysis of stranded electricity conductors in skew winds. Wind and Structures 11(4), 303-321.
- Madugula, M.K.S., 2002. Dynamic response of lattice towers and guyed masts. American Society of Civil Engineers, Reston, VA, USA.
- McCarthy, P., Melsness, M., 1996. Severe weather elements associated with September 5, 1996 hydro tower failures near Grosse Isle, Manitoba, Canada. Environment Canada, Winnipeg, Canada.
- Savory, E., Dalley, S., Toy, N., 1992. The effects of eaves geometry, model scale and approach flow conditions on portal frame building wind loads. Journal of Wind Engineering and Industrial Aerodynamics 41-44, 1665-1676.
- Shehata, A.Y., El Damatty, A.A., 2007. Behaviour of guyed transmission line structures under downburst wind loading. Wind and Structures 10(3), 249-268.
- Shehata, A.Y., El Damatty, A.A., 2008. Failure analysis of a transmission tower during a microburst. Wind and Structures 11(3), 193-208.
- Shehata, A.Y., El Damatty, A.A., Savory, E., 2005. Finite element modeling of transmission line under downburst wind loading. Finite Elements in Analysis and Design 42, 71-89.
- Zhu, N., 2007. Wind tunnel test for guyed mast dynamic characteristics under wind loads. University of Saskatchewan.

Table 1. Model scaling parameters.

Parameter	Scaling ratio
Global:	
length	$\lambda_L = 1E-02 = 1: 100$
wind speed	$\lambda_V = \lambda_L^{0.5} = 1E-01 = 1: 10$
time	$\lambda_T = \lambda_L / \lambda_V = 1E-01 = 1: 10$
Structure:	
density	$\lambda_p = 1E+00 = 1: 1$
mass per unit length	$\lambda_m = \lambda_L^2 = 1E-04 = 1: 10000$
mass	$\lambda_M = \lambda_L^3 = 1E-06 = 1: 1000000$
mass moment of inertia	$\lambda_I = \lambda_M \cdot \lambda_L^2 = 1E-10 = 1: 10000000000$
damping	$\lambda_c = 1E+00 = 1: 1$
axial rigidity	$\lambda_{EA} = \lambda_V^2 \cdot \lambda_L^2 = \lambda_L^3 = 1E-06 = 1: 1000000$
flexural/torsional rigidity	$\lambda_{EI} = \lambda_{GC} = \lambda_V^2 \cdot \lambda_L^4 = \lambda_L^5 = 1E-10 = 1: 10000000000$
force	$\lambda_F = \lambda_V^2 \cdot \lambda_L^2 = \lambda_L^3 = 1E-06 = 1: 1000000$
force per unit length	$\lambda_f = \lambda_V^2 \cdot \lambda_L = \lambda_L^2 = 1E-04 = 1: 10000$
bending/torsional moment	$\lambda_{BM} = \lambda_V^2 \cdot \lambda_L^3 = \lambda_L^4 = 1E-08 = 1: 100000000$

Table 2. Response spectral density components for boundary layer wind load.

Fig. 8	U at z = 0.345 m		m_{R1}^2 frequency band	
	(m/s)	m_B^2/m_T^2	m_{R1}^2/m_T^2	(Hz)
(a)	3.5	20%	47%	3.2 to 6.3
(b)	4.5	24%	38%	3.9 to 6.3
(c)	5.6	22%	33%	4.4 to 7.2
(d)	6.7	22%	23%	4.5 to 7.9
n/a	6.7	21%	30%	4.4 to 8.3

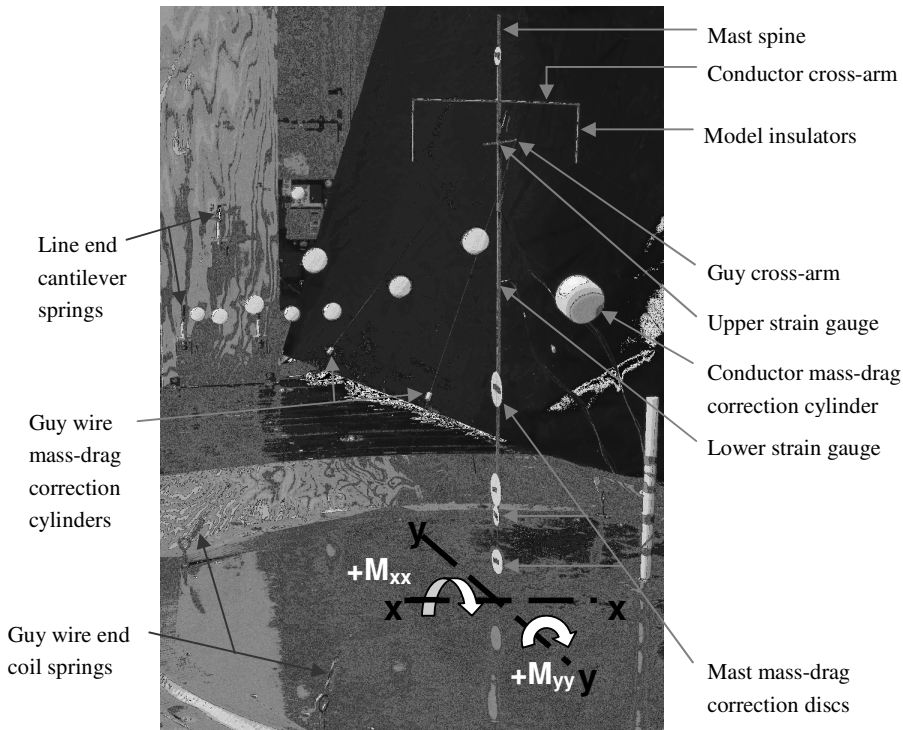


Figure 1. Assembled aeroelastic model.

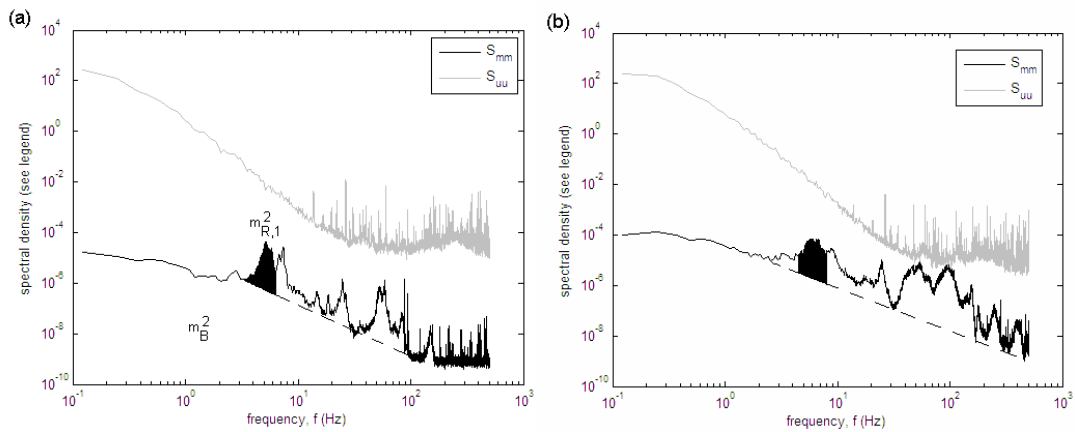


Figure 2. Boundary layer fluctuating wind speed and tower response spectra with a conductor-height mean wind speed of (a) 3.5 m/s and (b) 6.7 m/s.

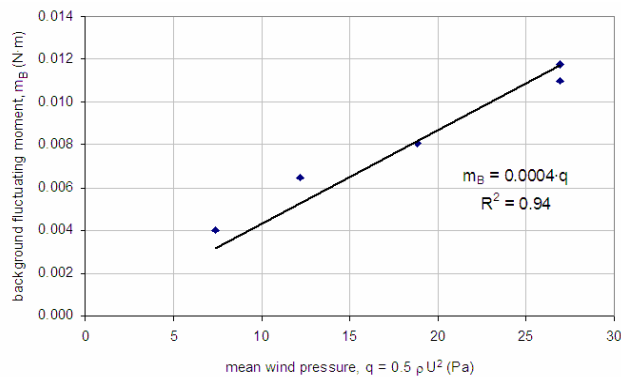


Figure 3. The variation of the background component of tower response with boundary layer mean wind pressure.

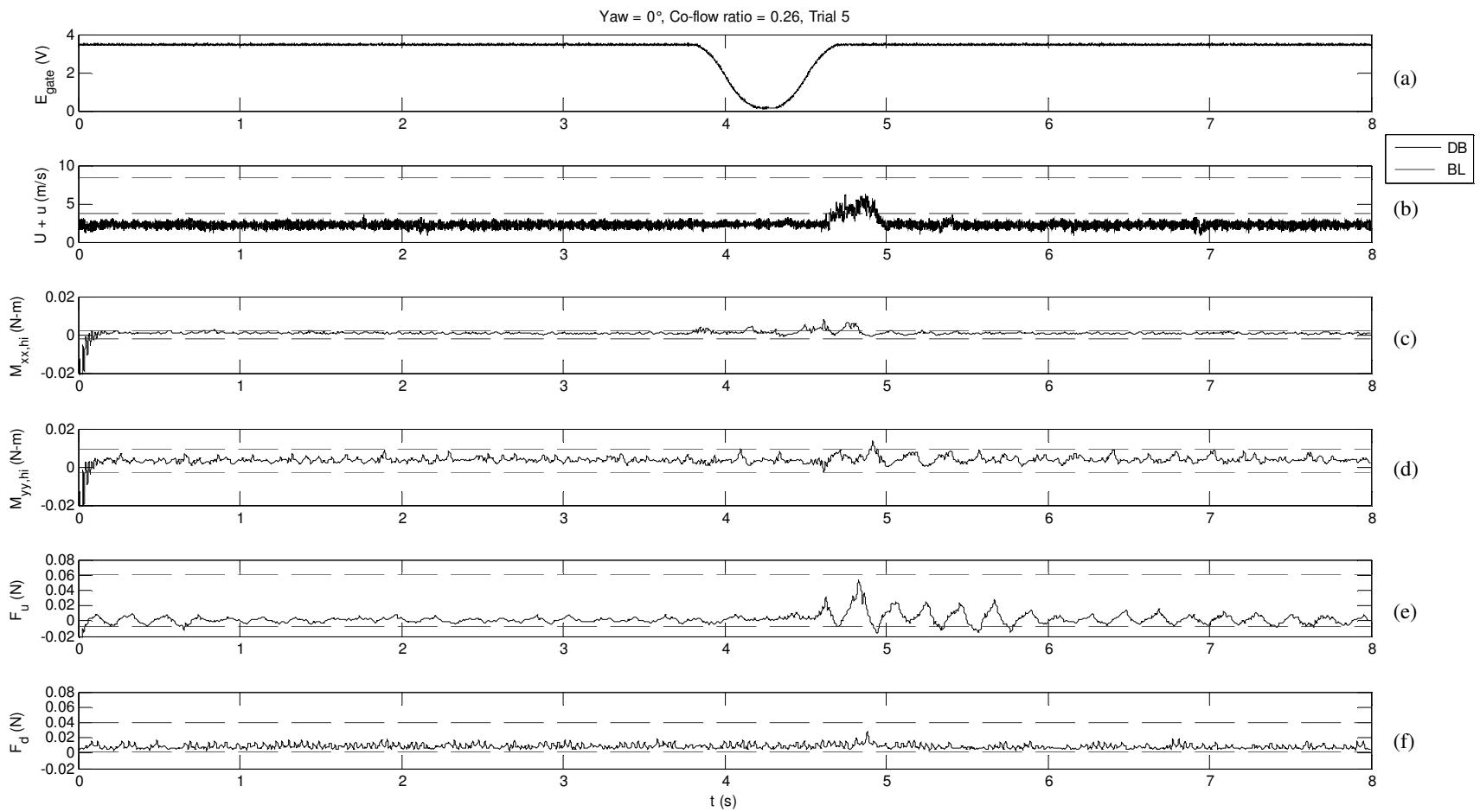


Figure 4. Synchronized histories of measured (a) slot gate position, (b) streamwise velocity, (c) spine bending moment about the x-x axis, (d) spine bending moment about the y-y axis, (e) upstream conductor axial force and (f) downstream conductor axial force.